International Journal of Heat and Mass Transfer 237 (2025) 126425

Contents lists available at ScienceDirect

International Journal of Heat and Mass Transfer

journal homepage: www.elsevier.com/locate/ijhmt

A novel method for fast and efficient numerical simulation of microwave heating in liquids during mixing

Bhupinder Singh [a,*], Samuel Hefford [b], Enrique Sanchez-Perez [c], Michael Barter [b], Daniel R. Slocombe [b], Serena A. Cussen [d], Georgios Dimitrakis [a,*]

[a] Department of Chemical and Environmental Engineering, University of Nottingham, University Park, Nottingham NG7 2RD, United Kingdom
[b] School of Engineering, Cardiff University, Park Place, Cardiff CF10 3AT, United Kingdom
[c] School of Chemical, Materials and Biological Engineering, University of Sheffield, Sheffield S1 3JD, United Kingdom
[d] School of Chemistry, University College Dublin, Belfield, Dublin 4, Ireland

ARTICLE INFO

Keywords:
Microwave
Temperature
Multi-physics modelling
Simulation
Frozen rotor
Mixing
Stirrer

ABSTRACT

Microwave-assisted chemical reactions present potentially more sustainable routes for process intensification compared with traditional approaches, due to the reduction of reaction times, temperatures, and side reactions. Despite the common misconception that microwave heating is uniform, many processes can be expected to show temperature distributions that vary significantly over the volume, even at length scales far below the operating wavelength. Numerical methods are often employed in the design and optimization phase of a given process, however, due to the multitude of interdependent physics required; the fast and efficient modelling of microwave heating in liquids remains a significant challenge, particularly with respect to computational resources. Here, we report a new multi-physics simulation methodology that models microwave heating of liquids during agitation, requiring less computational resources and delivering temperature predictions within 2.78 % of relative root mean square error. By applying the frozen rotor approach, near-perfect temperature profiles are predicted at approximately 600 times faster convergence time compared to the conventional sliding mesh method. Our proposed model can be used to mimic real reaction systems in a fast and resource-efficient way.

1. Introduction

The exploration of high-definition radar during the First World War heralded the advent of microwave frequency technology development. Broadly defined, microwaves refer to electromagnetic waves in the frequency range of 300 MHz to 300 GHz. Whilst, principally used for communication, the accidental discovery by Spencer in 1946 led to the development of microwave heating technology [1]. Since then, there have been many studies devoted to understanding the phenomenon of heating materials via microwave energy [2–5]. Of the possible loss mechanisms, dipolar heating and conduction heating have been mostly explored. Finding the accelerated reaction kinetics due to dipole polarisation by the oscillating electromagnetic field opens new prospects in chemical engineering.

Microwave-assisted reactions have shown promise for use in materials synthesis as well as process intensification applications offering higher yields, reduced reaction times, and safer operations [6–8]. Microwave heating resulting from the interaction of electromagnetic radiation with ions and molecules leads to rapid and selective heating [9]. This characteristic makes microwaves a promising technology for applications in many fields of chemical engineering, including, distillation, crystallization, extraction, drying, reaction processes (esterification), chemical catalysis, organic synthesis, and polymerization [10–13]. Significant research has been conducted in these fields, highlighting the advantage of microwave-assisted reactions over conventional counterparts. For instance, Baker-Fales et al. showed enhanced extraction efficiency and volumetric mass transfer coefficients with microwave processing [14]. Vidal Laveda et al. have reported the application of microwave heating for the preparation of olivine structured $LiFe_{1-x}Mn_xPO_4$ cathodes. This study demonstrates that microwave heating offers a faster route to olivine structured cathodes. In addition to this, total scattering measurements have shown that fewer crystallographic defects manifest during microwave synthesis, compared with traditional solvothermal approaches, which directly influences the resulting electrochemical performance of these cathodes in battery cells [15]. These encouraging results suggest that microwave heating offers a

* Corresponding authors.
E-mail addresses: bhupinder.singh@nottingham.ac.uk (B. Singh), georgios.dimitrakis@nottingham.ac.uk (G. Dimitrakis).

https://doi.org/10.1016/j.ijheatmasstransfer.2024.126425
Received 13 August 2024; Received in revised form 18 October 2024; Accepted 5 November 2024
Available online 12 November 2024

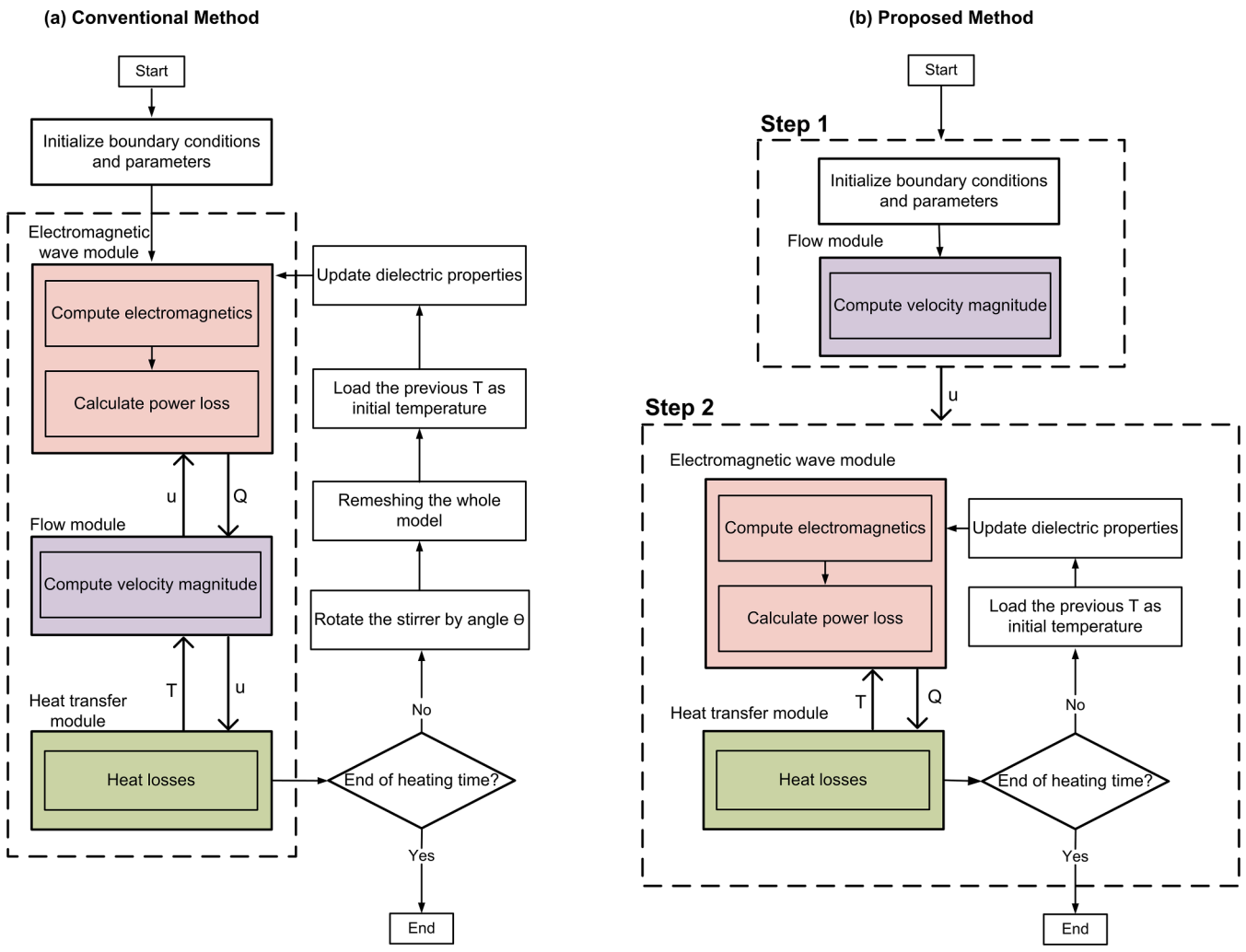

Fig. 1. Steps involved in the (a) conventional and (b) proposed model for describing microwave heating in liquids.

promising alternative route to generating high quality energy storage materials. Beside the energy-intensive process, microwave heating has excellent potential to achieve a negative carbon footprint as microwaves run solely on electricity, which can potentially be sourced from renewable sources.

Despite the widely reported successes in academic discourse; microwave heating languishes on its way to the chemical industry as a result of uneven heating. This uneven heating arises from the non-uniform dielectric content of the reactant feedstock itself, where different materials will exhibit wildly different values for permittivity, resulting in localised field changes [16]. Other than this, in the case of liquid heating, fluid flow plays a vital role in the distribution of temperature inside the liquid [17]. Therefore, flow information should be considered during designing microwave reactors for chemical reactions. The use of mathematical modelling and simulation could be a powerful tool, providing valuable insight into the factors affecting the temperature inside the reaction vessel and guiding the design of microwave reactors for uniform heating.

Previous reports on the simulation of batch microwave heating of liquids demonstrate the challenges of non-uniform heating in the liquid state [18–21]. The liquid flow associated with batch processing is via convection only. For this reason, continuous flow reactions were introduced which delivers better heating efficiency attributed to forced flow which affords better microwave absorption [22–25].

Most existing microwave chemical processes apply single-mode reactors, which feature built-in magnetic stirrers or alternative agitation devices, and direct temperature control of the reaction mixture. Agitation of the liquid during microwave heating diffuses the heat generated, thereby diluting the hot spots. The numerical simulation of such a heating process in microwave reactors with a stirrer is challenging. The challenges lie in physical modelling, computer requirements, computational time, and numerical stability. These issues developed as a result of the complex geometry of the impeller, rotation of the impeller and consequent turbulence, and, most importantly, multi-physics calculation of the microwave heating of the stirred liquid, demanding the coupling of electromagnetics, temperature, and velocity fields. Previously demonstrated models used to toggle between simulation steps to adjust the sample position, ensuring its complete rotation within the microwave cavity [26]. Other than this, alternative methods that use moving wall conditions under flow physics have been reported to obtain a continuous rotation [27]. This method requires remeshing during the motion and therefore applied to simple geometries like cylindrical vessels rotating on their central axis to avoid mismatching of the mesh. Its application with irregular geometries such as a rotating impeller inside the vessel may cause convergence challenges due to the high computational demand. Here, we directly address this challenge by presenting a 3D model for the fast and efficient simulation of microwave heating in stirred liquids. Our proposed model will reduce the computational resource required by using a frozen rotor approach while still predicting near-perfect temperature profiles. Our 3D simulation model is validated against experimental data with relative root mean square error (RRMSE) representing the model efficacy. We implement our new model to

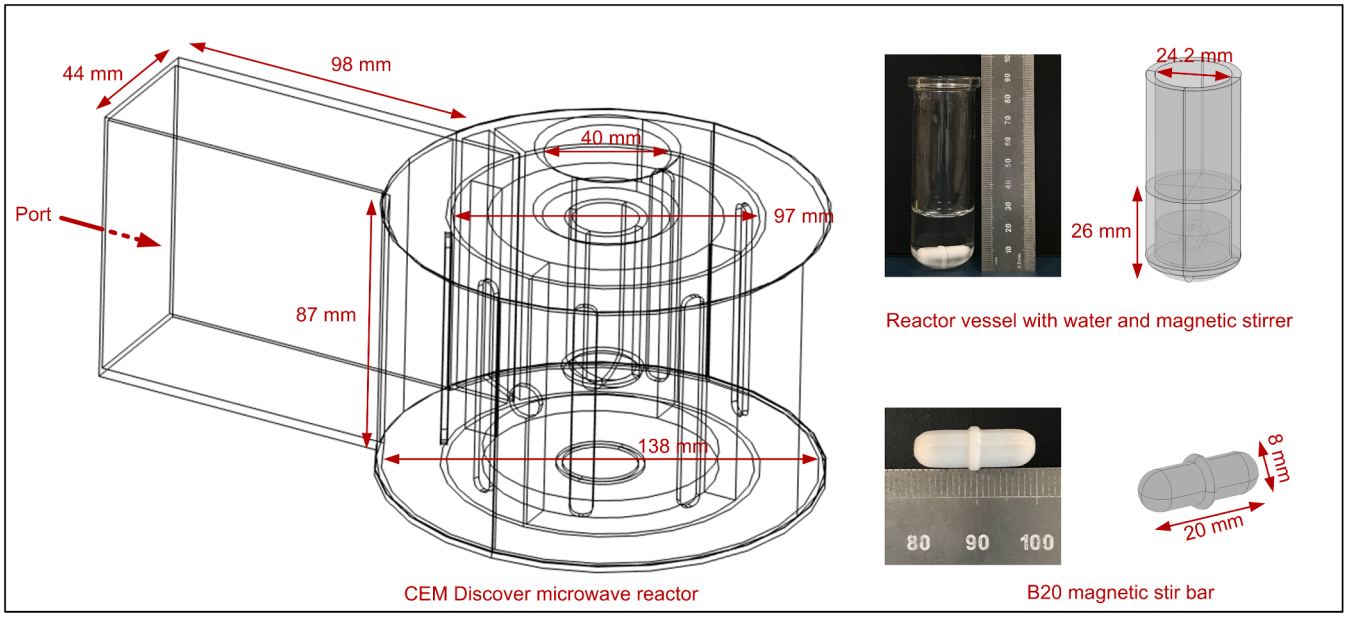

Fig. 2. Geometric model of CEM Discover microwave applicator, reactor vessel, and stirrer.

demonstrate the stirring effect for liquids. We also examine the effect of microwave input power on the coefficient of variation (COV) and microwave power absorption. Finally, the impact of volume on E-field distribution and temperature rise was presented with experimental measurements.

2. Experimental procedure

A commercially available CEM Discover single-mode microwave reactor was used for experimental trials. The reactor, operating at 2.45 GHz, has a discrete and adjustable power setting, up to 300 W using integrated computer software. A 35 mL sealed pressure vessel containing the target material was placed in the centre of the cylindrical cavity. The vessel has a PTFE-coated magnetic stirrer for efficient mixing of the liquid during microwave heating. The waveguide consists of a circular section that encircles the cavity and a rectangular section connected to a magnetron. The six slotted openings in the inner cavity wall facilitate the transmission of microwaves from the waveguide into the cavity [28]. The temperature of the sample was measured using a floor-mounted IR sensor. In the present study, water was used as a test fluid. The stirring speed was set to 600 rpm during the heating of the water.

3. Numerical simulation

The proposed mathematical model was developed to evaluate the microwave heating in liquids under stirring using the COMSOL Multiphysics 6.1 software tool. A Lenovo workstation with 32-GB RAM, Intel (R) Xeon(R) W-2223 CPU with 3.60-GHz processor was employed for this study. The computation time was 128 s to compute 1 s of microwave heating in stirred liquid, whereas the conventional method would take 80,000 s for the same computation. This significant discrepancy arises from the fact that the conventional method, working on a fully coupled approach, require mesh reconstruction. Operating with coupled physics restricts the ability to customize meshes at consecutive steps of the study, leading to excessive computational power demand. Therefore, choosing the right modelling approach is necessary depending on the nature of the problem, available computational resources, and desired accuracy. Our proposed method addresses several challenges presented by the conventional method considering all these factors. The current model illustrates the propagation of electromagnetic waves, temperature distribution, and fluid flow inside the reactor vessel. The computational steps involved in the simulation are shown in Fig. 1. The calculation is divided into two steps. In the first step, velocity fields are determined using a frozen rotor approach via the Flow module. The frozen rotor is a steady-state approach that assumes a fully developed flow, eliminating the need for multiple steps to establish the flow pattern. This allows the use of a discrete-step solution that can be imported into the second study step. The steady flow modelling using a frozen rotor is a widely practiced method in many engineering applications [29,30]. Researchers found it a more efficient method for predicting stirring in tank reactors than the conventional sliding mesh method [31–33]. The frozen rotor uses Reynolds-averaged Navier–Stokes equations (RANS) equations to provide a time-averaged description of fluid flow and therefore, are often easier to validate against experimental data. Subsequently, the derived solution from step 1 is utilized in step 2 where the Electromagnetic module is coupled with the Heat Transfer module for the prediction of temperature distribution in the vessel for the corresponding flow conditions. The details related to the physics of each module are further described in Section 3.3. The proposed method significantly improves computational efficiency and reduces computation time.

Table 1
Temperature-dependent dielectric properties of water [22].

Temperature (°C)	Relative complex permittivity
20	78.0 − *j*10.5
30	75.0 − *j*8.6
40	72.0 − *j*6.7
50	69.0 − *j*5.1
60	66.2 − *j*3.8
70	63.9 − *j*3.3
80	62.7 − *j*3.1
90	62.3 − *j*3.0
100	62.0 − *j*2.9

3.1. Model assumptions

The model assumptions were defined as follows to reduce the complexity and improve the convergence rate.

- Microwave waveguide is made of stainless steel.

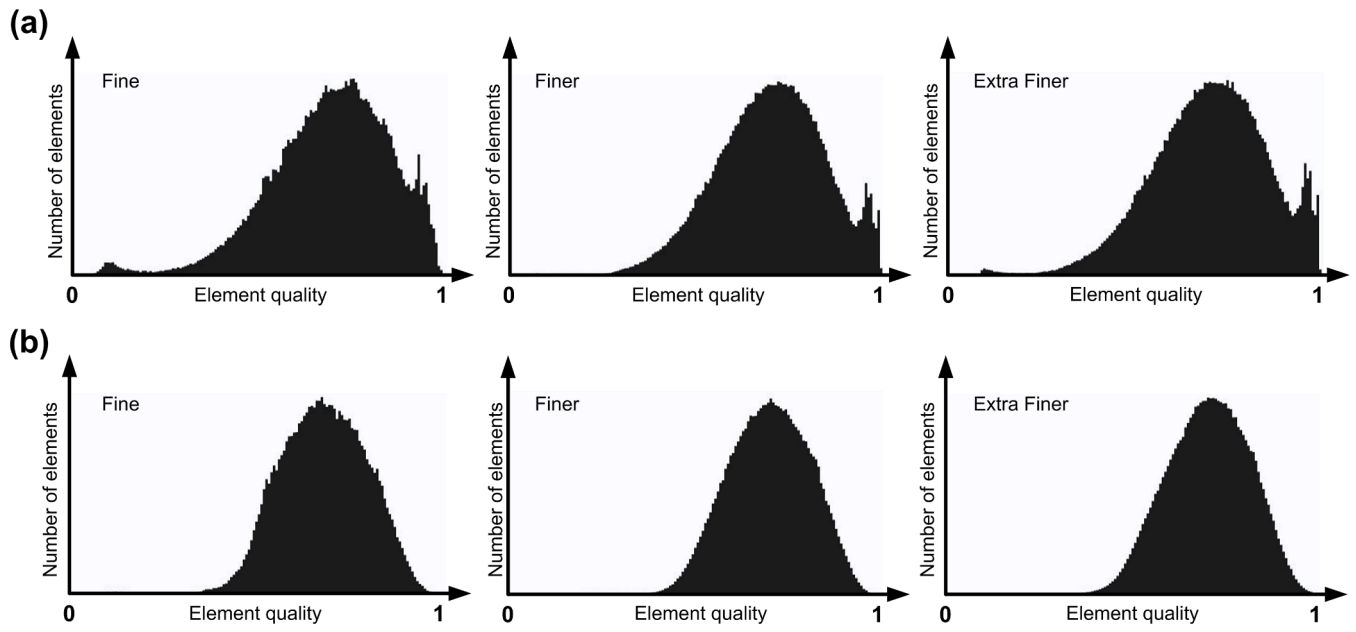

Fig. 3. Comparison of element quality for different element sizes (a) unstirred and (b) stirred liquid model.

- Assuming negligible microwave energy absorption by the air domain and that the medium is fully transparent for the propagation of microwaves.
- The system was initially at 24 °C.
- No phase transitions were considered during heating, as it was evaluated in advance and ruled out as unlikely for the system under study.
- The surface roughness of the reactor vessel was neglected.
- The fluid is incompressible.

3.2. Geometry

The 3D geometric model consisted of a metallic waveguide, a cylindrical cavity, and a PTFE stirrer inside the reactor vessel as shown in Fig. 2. The empty space in the waveguide was filled with air. A standard WR340 waveguide was excited with the TE_{10} mode, which is the dominant mode in the 2.45 GHz frequency. The geometric parameters of the reactor vessel along with its physical model are shown in Fig. 2. Pyrex glass was incorporated as vessel material. The vessel was filled with deionised water up to a level of 26 mm. Table 1 represents the temperature-dependent dielectric properties of the water enforced in the model [22].

3.3. Governing equations

3.3.1. Flow

The current model predicts flow fields in the reactor vessel using the frozen rotor technique. The frozen rotor, also referred as the moving reference plane, divides the domain of interest into a rotating domain and a static domain. Unlike the sliding mesh approach, the relative position between the rotating domain and the static domain remains constant. The methods solve momentum equations for the stationary and the rotating system individually, using Eqs. (2) and (3), respectively [34]. The Continuity equation is given by:

$$\rho\nabla.(\boldsymbol{u}) = 0 \tag{1}$$

We define the momentum equation for the static system as:

$$\rho(\boldsymbol{u}.\nabla)\boldsymbol{u} = \nabla.\left[-pI + \mu\left(\nabla\boldsymbol{u} + (\nabla\boldsymbol{u})^T\right)\right] + \rho g \tag{2}$$

and for the rotating system as:

$$\rho(\boldsymbol{u}.\nabla)\boldsymbol{u} = \nabla.\left[-pI + \mu\left(\nabla\boldsymbol{u} + (\nabla\boldsymbol{u})^T\right)\right] + \rho g + F \tag{3}$$

where, F is the source term for Coriolis and centrifugal force, ρ is the density, T is the temperature, $\boldsymbol{u}$ is the velocity, I is the unit matrix and μ is the viscosity.

3.3.2. Electromagnetic

The Helmholtz equation, which governs electromagnetic distribution, was solved for the whole computational geometry and can be expressed as follows:

$$\nabla^2 E + \varepsilon_r\left(\frac{2\pi f}{c}\right)^2 E = 0 \tag{4}$$

where, E is the electric field at an angular frequency of $\omega = 2\pi f$ and c is the speed of light. Here, the relative permittivity (ε_r) dominates the level of heat generation inside the dielectric material and can be further expressed as [35]:

$$\varepsilon_r = \frac{\varepsilon' - j\varepsilon''}{\varepsilon_0} \tag{5}$$

where, the real part of the permittivity, ε', is termed the dielectric constant and represents the amount of electric energy stored inside the exposed material. The imaginary part, ε'', represents the ability of a material to convert this energy into heat and is called dielectric loss. The imaginary part accounts for various mechanisms of energy loss, most notably the flow of electric current inside the material, which is closely related to penetration depth (δ). Therefore, microwaves cannot penetrate in the similar fashion in all the material. The penetration depth of the material can be calculated from the equation [36]:

$$\delta = \frac{c}{\sqrt{2}\pi f\left[\varepsilon'\left\{\sqrt{1 + \left(\frac{\varepsilon''}{\varepsilon'}\right)^2} - 1\right\}\right]^{1/2}} \tag{6}$$

Therefore, the microwave power (P_d) will be attenuated as the electromagnetic fields penetrate the material and can be expressed as follows [2]:

$$P_d = \frac{1}{2}\omega\varepsilon_0\varepsilon''|E|^2 \tag{7}$$

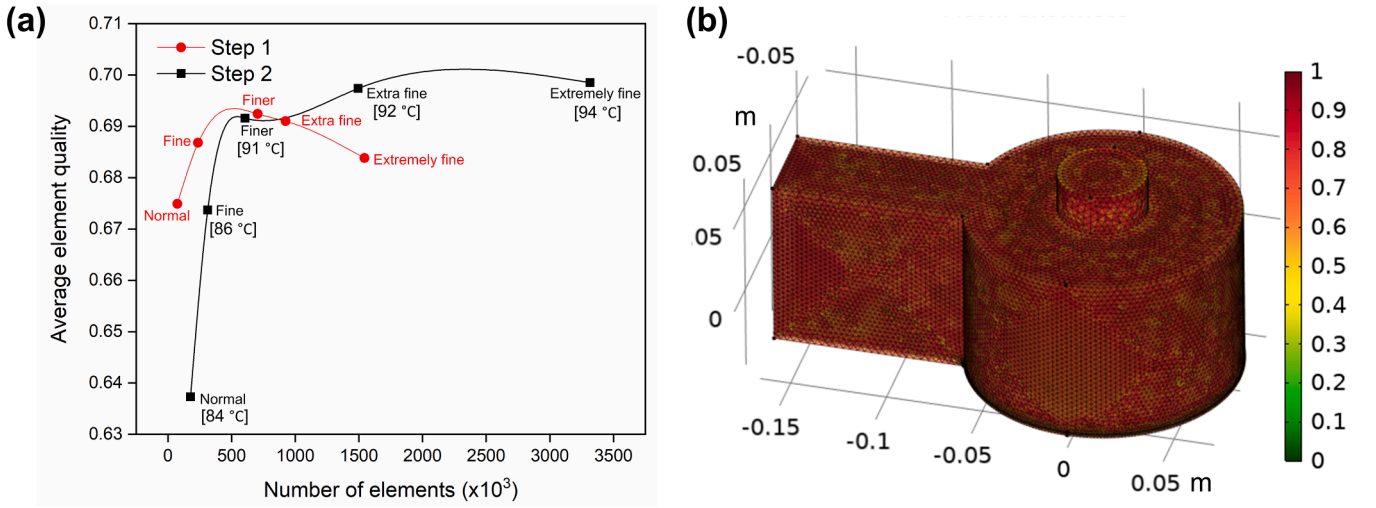

Fig. 4. (a) Influence of mesh size on average element quality [Parentheses shows change in Final temperature of the water with number of elements], (b) Mesh quality statics for finer mesh used.

It is worth mentioning that dielectric properties change with temperature and therefore the change in the field distribution must also be considered over time. The COMSOL Multiphysics software applied here affords us a means to do this.

3.3.3. Heat transfer

The heat transfer equation, Eq. (8), was solved to obtain the temperature distribution [37].

$$\rho c_p \frac{\partial T}{\partial t} + \rho c_p \boldsymbol{u}.\nabla T = \nabla.(k\nabla T) + P_d \tag{8}$$

where, P_d describes the heat source, T is the temperature, k is the thermal conductivity and c_p is the heat capacity.

3.4. Boundary conditions

In the flow module, a no-slip condition ($\boldsymbol{u} = 0$) was applied to the walls of the vessel and stirrer, whereas slip conditions ($\boldsymbol{n}.\boldsymbol{u} = 0$) were implemented at the liquid surface level to replicate a free surface. In an electromagnetic module, an impedance boundary condition imposed on metal walls of microwave cavity ensures no microwave leakage, and can be expressed as [35]:

$$\sqrt{\frac{\mu_0\mu_r}{\varepsilon_0\varepsilon_r - j\frac{\sigma}{\omega}}}\boldsymbol{n} \times H + E - (n.E)n = (n.E_s)n - E_s \tag{9}$$

where, H is the induced magnetic field and E_s is the tangential component of the electric field. The current model considers convective and radiative heat loss effecting the temperature of the liquid. These heat losses were taken into account by applying heat flux boundary conditions as described below [35]:

$$-\boldsymbol{n}.(-k\nabla T) = h(T_0 - T) + \varepsilon_{rad}\sigma\left(T_0^4 - T^4\right) \tag{10}$$

where, T_0 is the ambient temperature, ε_{rad} is the surface emissivity of glass taken as 0.84, σ is the Stefan–Boltzmann constant (5.67×10^{-8} W m^{-2} K^{-4}), and h is the natural convective heat transfer coefficient, taken as 10 W/(m^2 K).

3.5. Mesh size

As mentioned earlier, our model was converged in two discrete steps, step 1 and step 2, where substantially different physics are applied for

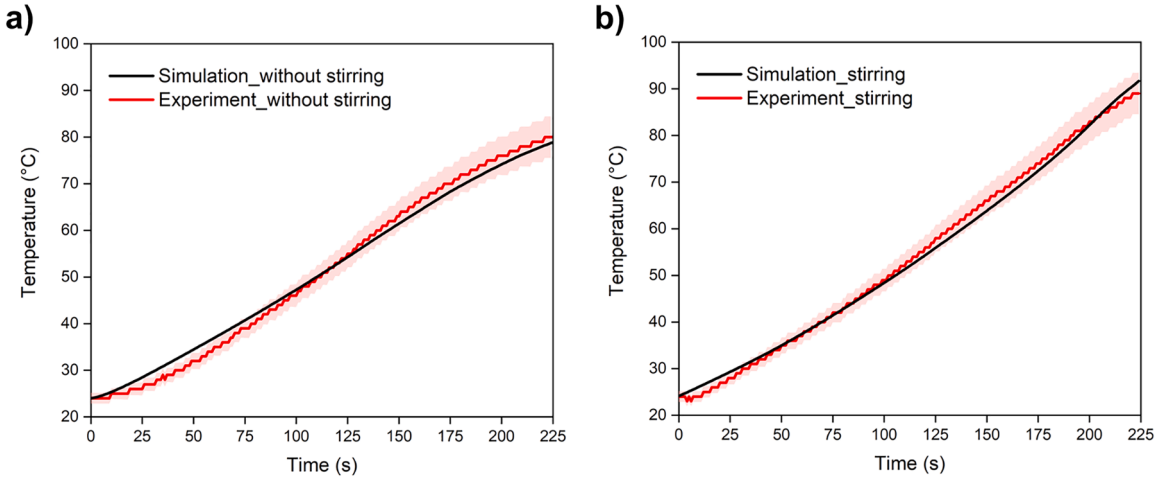

Fig. 5. Temperature prediction in (a) unstirred and (b) stirred water domain.

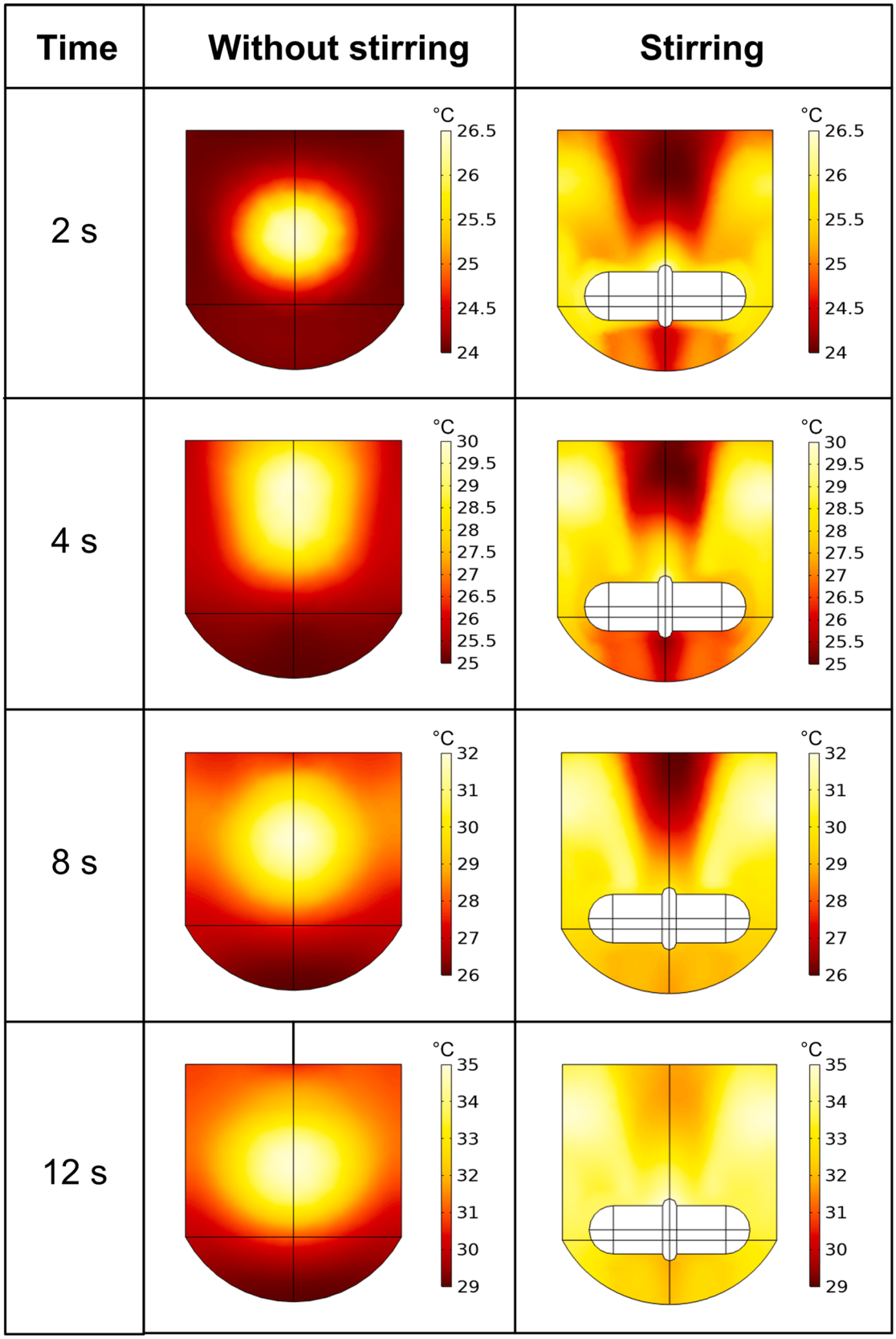

Fig. 6. Temperature contours of the simulated water domain at various time intervals.

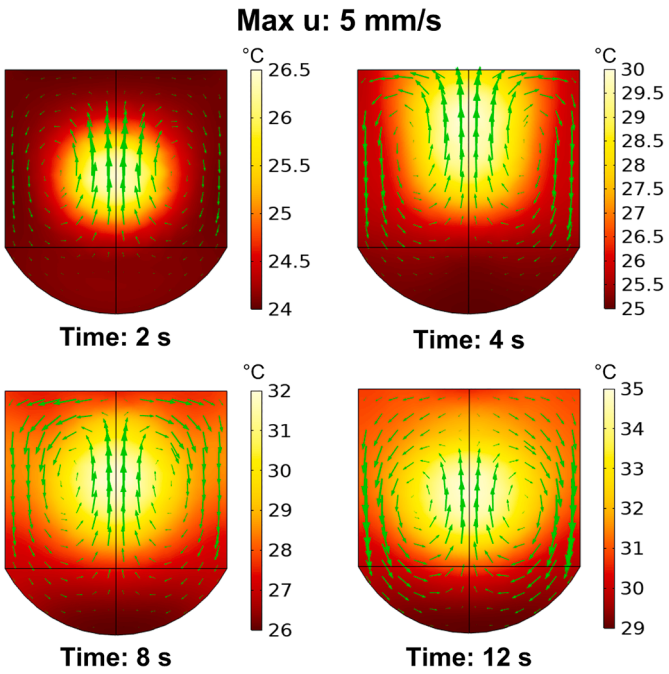

Fig. 7. Temperature contour and velocity fields in the unstirred sample at various time intervals.

each. A complementary mesh independent study was performed separately for the individual steps. The user defined mesh with free tetrahedral element type was selected. The element size was calibrated by examining the mesh quality under normal, fine, finer, extra fine, and extremely fine mesh size. Fig. 3 shows statistical graph between element quality and number of elements under fine, finer, and extra fine mesh size. On the *x*-axis, which describes the element quality, a value of 0.0 represents a degenerated element while 1.0 represents a completely symmetric element. Analysis of these data (Fig. 4(a)) demonstrates that a finer mesh produces the most accurate prediction of the final temperature of the target liquid, closely matching the experimental measurement. This mesh, with its optimal element quality, has therefore been taken into consideration for further simulations. The mesh quality statistics for a finer mesh (shown in Fig. 4(b)) are representative of a good-quality mesh.

4. Results and discussion

4.1. Model validation

The temperature measured during experiments was compared with simulation results to validate the model. Three sets of experiments were performed at 40 W microwave power with and without water stirring. The experimentally measured temperature values with a 5 % error band are plotted in Fig. 5, together with simulation results for the transient temperature at the bottom of the vessel. Fig. 5 shows good agreement between experimentally measured values and simulation results.

The performance of the model was evaluated quantitively by using the relative root-mean-square error (RRMSE). The use of RRMSE is a widely used metric for evaluating numerical models [38,39]. RMSE measures the average difference between the simulated and experimental results as shown in Eq. (11):

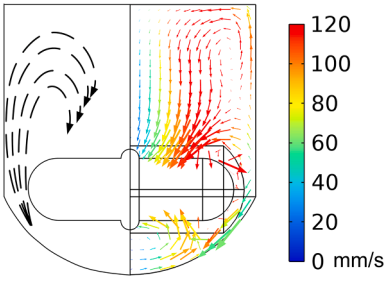

Fig. 8. Velocity field in the sample as a result of rotating stirrer.

$$\text{RRMSE} = \frac{\sqrt{\frac{1}{m}\sum_{i=1}^{m}(T_s - T_e)^2}}{\frac{1}{m}\sum_{i=1}^{m}T_e} \times 100 \tag{11}$$

where, T_e and T_s are the experimental and simulated temperature values respectively, and m denotes the data points. The RRMSE was found to be 3.04 % for unstirred and 2.78 % for stirred samples. The higher RRMSE value for the unstirred case can be attributed to the challenge of pinpointing the location on the vessel for extraction of simulation results. This is due to the fact that the non-contact type pyrometer utilized by CEM Discover does not allow the determination of the exact point of temperature measurement. However, considering the location of the IR sensor in CEM Discover, the bottom point of the vessel was chosen for extracting the simulation results. This situation is different in the stirred case as it has almost the same temperature at every point, which is further discussed in detail in Section 4.2. Furthermore, the assumptions made in the flow module as stated in Section 3.1. might have introduced errors in the simulation results. Nevertheless, the RRMSE values indicate that model predictions are reasonably accurate and thus it can be used to

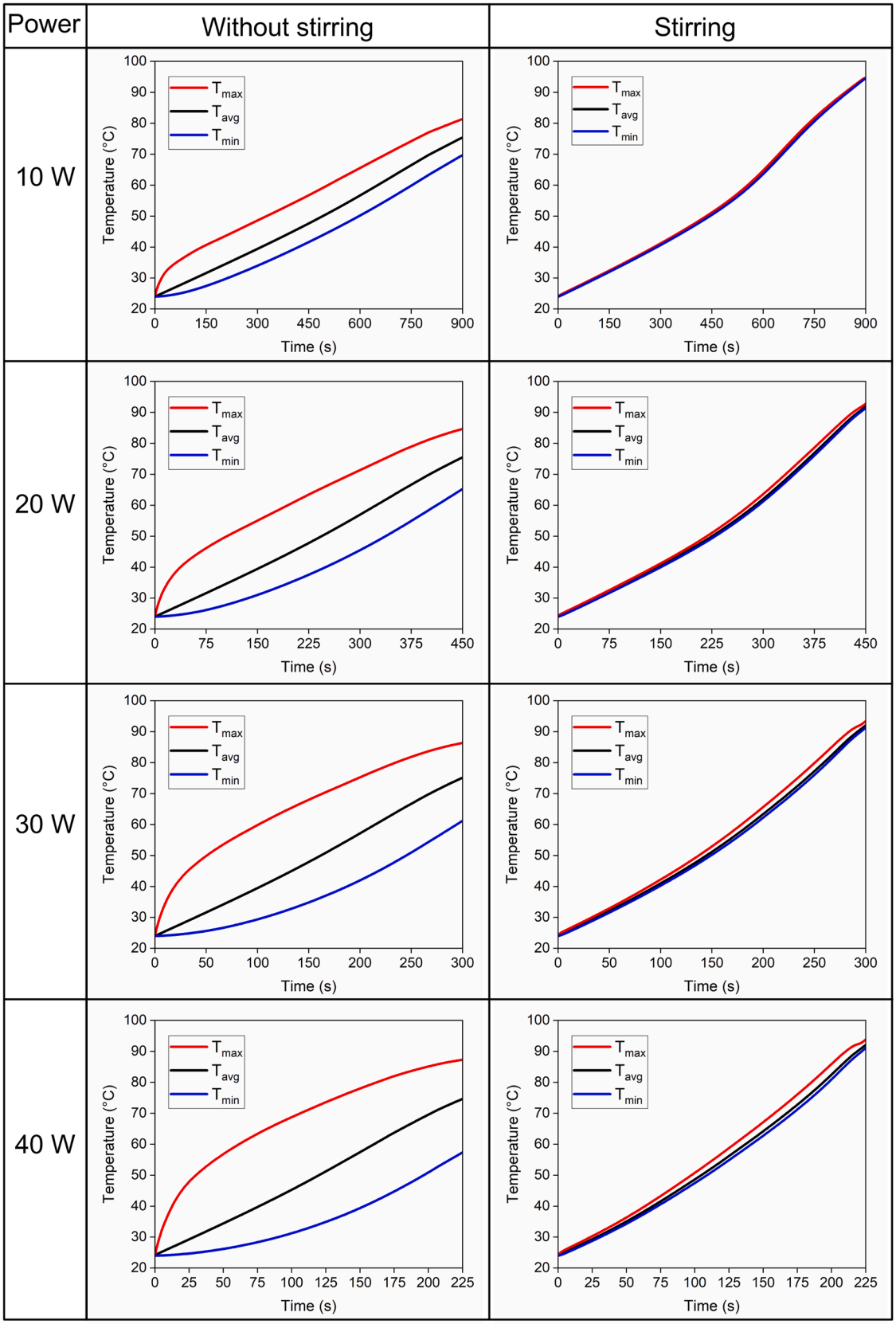

Fig. 9. Influence of input power on simulated T_{max}: maximum temperature, T_{avg}: average temperature and T_{min}: minimum temperature of unstirred and stirred water.

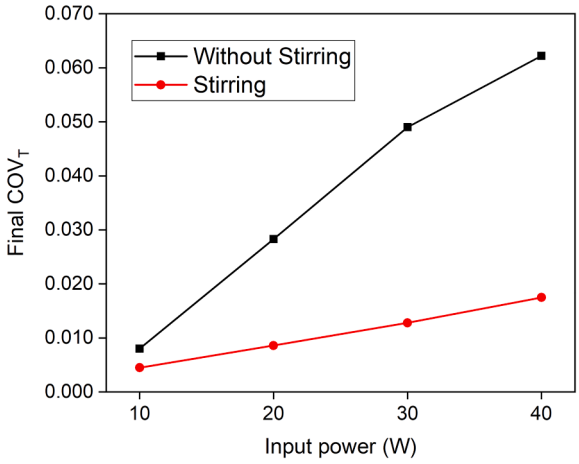

Fig. 10. COV_T values under different input power.

simulate microwave heating in liquids even under agitated conditions.

4.2. Effect of stirring

Microwave heating is significantly influenced by the penetration depth and the dielectric properties of the liquid. A consequence of this is the likelihood of hot and cold spots within the sample. The current model aims to illustrate the effect of stirring on achieving uniformity in microwave heating. Fig. 6 represents the temperature contour of liquid with varying microwave exposure times, ranging from 2 s to 12 s, both with and without stirring. The initial temperature contour reveals higher temperature in the core of the liquid, with colder regions near the reaction vessel walls. This can be explained based on the higher microwave penetration depth in water [40]. Furthermore, the implied stirring in the numerical model predicts an even temperature distribution compared to the non-stirred liquid. The non-stirred model considers natural convective heating due to temperature difference (Fig. 7). Clearly, the convective currents alone were found to be insufficient for attaining uniform heating. Therefore, the occurrence of non-uniform temperatures in microwave reactor is highly apparent in the absence of liquid stirring.

Further, the predicted velocity field within the reactor vessel as a result of stirring, as shown in Fig. 8, indicates that flow in the lower region is suppressed, resulting in an axially asymmetric flow. In case of magnetic stirrer, there is a hydrodynamic obstacle that is imposed by the limited clearance between stirrer and bottom of the vessel which constraints the formation of fully developed axial flow. This observation is in agreement with a previous study reporting the dependency of hydrodynamics on clearance [33,41]. The present model reveals that peak mean velocity originates in the vicinity of the stirrer, and decreases towards the tank wall, redirecting an upward inclination of the fluid near the wall and downward liquid motion towards the centre. Though, natural convection is indeed present in the reactor during stirring. The stirring force generated by the stirrer is sufficiently large to dominate over the natural convection effect. Furthermore, the model simulates the CEM Discover system, where the lowest rpm possible is 400. Such high rpm far exceeds the velocity field associated with natural convection; therefore, natural convection is not considered in the stirring case. The difference in velocity field due to natural convection and stirring can be seen in Figs. 7 and 8.

Table 2
Change in absorbed power with input power with and without stirring.

Input power (W)	Absorbed power (W)	
	Without stirring	With stirring
10	1.50885	2.10261
20	3.04645	4.21865
30	4.66028	6.31924
40	6.28019	8.43120

4.3. Effect of power

Reduced reaction times leading to enhanced productivity and faster turnaround times are crucial in the context of process intensification. Microwave power is one of the process parameters that influences temperature rise which in turn affects the reaction rates of reactive processes [42]. In the present study, four different power patterns (10 W × 900 s, 20 W × 450 s, 30 W × 300 s, and 40 W × 225 s) delivering a fixed input energy of 9 kJ is imposed while studying the effect of microwave power on the resulting temperature profile. In addition to monitoring the temperature rise rate, uniform heating is also an important aspect of microwave-based heating, and can be quantitatively described by the coefficient of variation (COV_T) [43]:

$$COV_T = \frac{\sqrt{\frac{1}{m}\sum_{m}^{1}(T_i - T_a)^2}}{T_a} \tag{12}$$

where, m represents the measured data points, T_a is the average temperature and T_i is the instant temperature at a point in the liquid domain. A smaller COV_T value represents more uniform heating. The simulated temperature profiles at different power levels are shown in Fig. 9.

In the unstirred liquid, almost similar average volumetric temperatures (75.36–74.63 °C) were achieved with different input powers however, the final COV_T (0.008–0.062) differs significantly as represented in Fig. 10. It was observed that COV_T increases with an increase in power. It can be concluded that even though more input power could reduce the overall heating time, this results in poorer temperature uniformity. With stirring, the average temperature of water rises to 92.10 °C, and COV_T is reduced to 0.004 at 40 W microwave power. The stirred liquid exhibited a higher average temperature of 12–15 °C compared to the non-stirred liquid depending upon the power input. According to Eqs. (7) and (8), heat generation is a function of the electromagnetic power loss density. Therefore, this increase in average temperature compared to non-stirred liquid can be attributed to a change in absorbed power, which was determined by volume integration of the electromagnetic power loss density and is shown in Table 2. The results demonstrate that the absorbed power increases with stirring for each power setting. Further detailed analysis reveals that the electromagnetic power loss density was found to be strengthened in the central zone of the simulated water domain (Fig. 11). This suggests that the central zone has been exposed to higher microwave energy, potentially leading to higher heat generation. This is true for both stirred and unstirred cases; although, power absorption is likely to reduce when this central thermal zone does not diffuse as observed for the unstirred liquid domain, shown in Fig. 6. This is due to the temperature dependency of dielectric properties controlling power absorption as per Eq. (7). This also underscores the importance of controlling the temperature variation across the whole sample volume while working with microwaves. In a nutshell, model predictions indicated that improved heating uniformity can lead to a better heating rate.

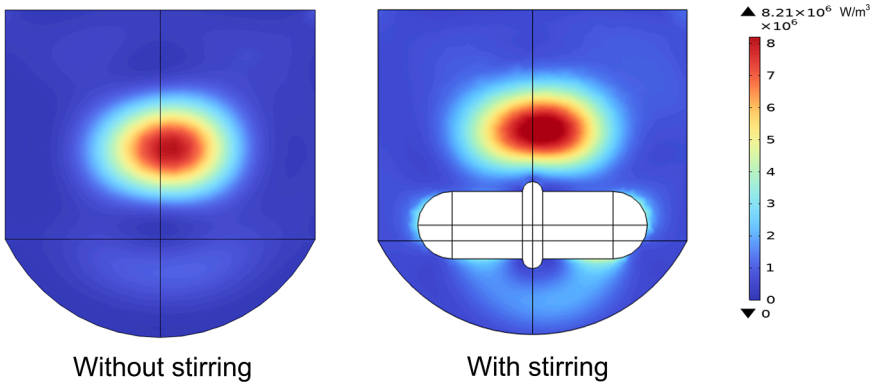

Fig. 11. Microwave power density inside the water domain at 40 W input power.

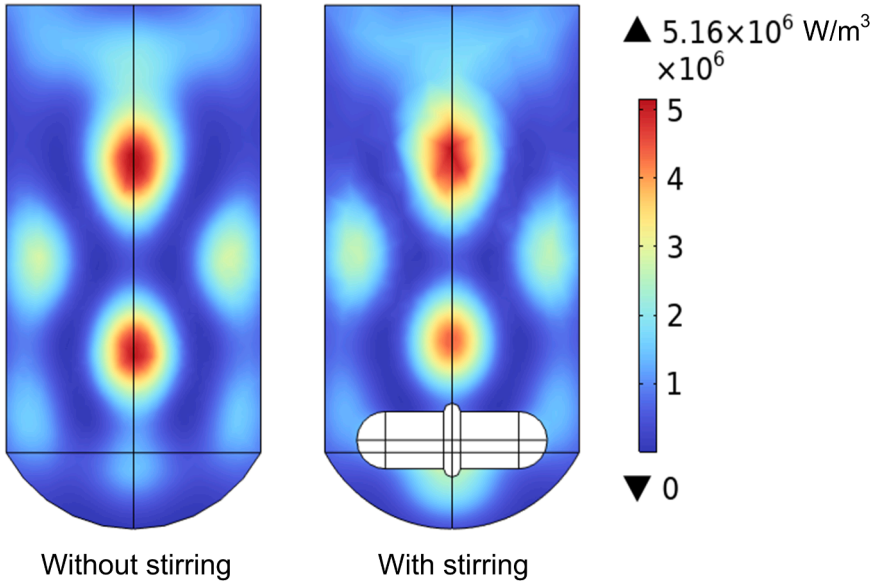

Fig. 12. Microwave power density inside the water filled to a height of 40 mm.

4.4. *Effect of volume*

In this section, the accuracy of the model is assessed by examining its prediction capability under varying load conditions within the cavity. The height of the water domain is increased to the level of 40 mm under both stirred and non-stirred conditions. Introducing a material with a high dielectric constant and dielectric loss into a microwave cavity alters the electric field distribution. The same is predicted by the model in Fig. 12 for the water. The increase in volume of water further perturbs the field distribution, resulting in a shift in the energy absorption pattern. The peak of electric field loss is no longer in the center of the load. This effects the temperature distributions for stirred and non-stirred liquids as presented in Fig. 13. A similar pattern of temperature distribution was observed experimentally by Sturm et al. for non-stirred water in CEM Discover [21]. The temperature uniformity improves for the stirred liquid. For both water volumes, the simulated temperature profiles are within 5 % error bar of experimental results (Figs. 5 and 14), this emphasizes model's ability to predict temperature distribution under varying loads. This confirms its reliability and robustness in scenarios involving substantial changes in dielectric material in the cavity.

5. Conclusions

A new and fast Multiphysics model that simulates microwave heating of liquids in an agitated state shows that the temperature rise in the liquid is significantly influenced by microwave power. A higher microwave power leads to a higher heating rate, but there is a trade-off in non-uniform temperature distribution inside the reactor vessel. Our simulation results suggest that temperature uniformity can be enhanced by stirring, shown quantitatively via the coefficient of variation (COV_T). The maximum COV_T was found to be 0.062 without stirring at 40 W input power, decreasing substantially to 0.004 with stirring for a water load in a vial filled up to a height of 26 mm. Our analysis of distributions of electromagnetic power loss density, and temperature demonstrated that stirring within the reactor vessel is essential not just for ensuring temperature uniformity but also for regulating the volume temperature of the liquid. Our model demonstrated that stirring increases the final average temperature by 12–15 °C compared to the non-stirred liquid. Further, analysis showed that the volume of load inside the cavity has a significant impact on the electric field distribution.

In summary, the model can be used to predict the temperature profile

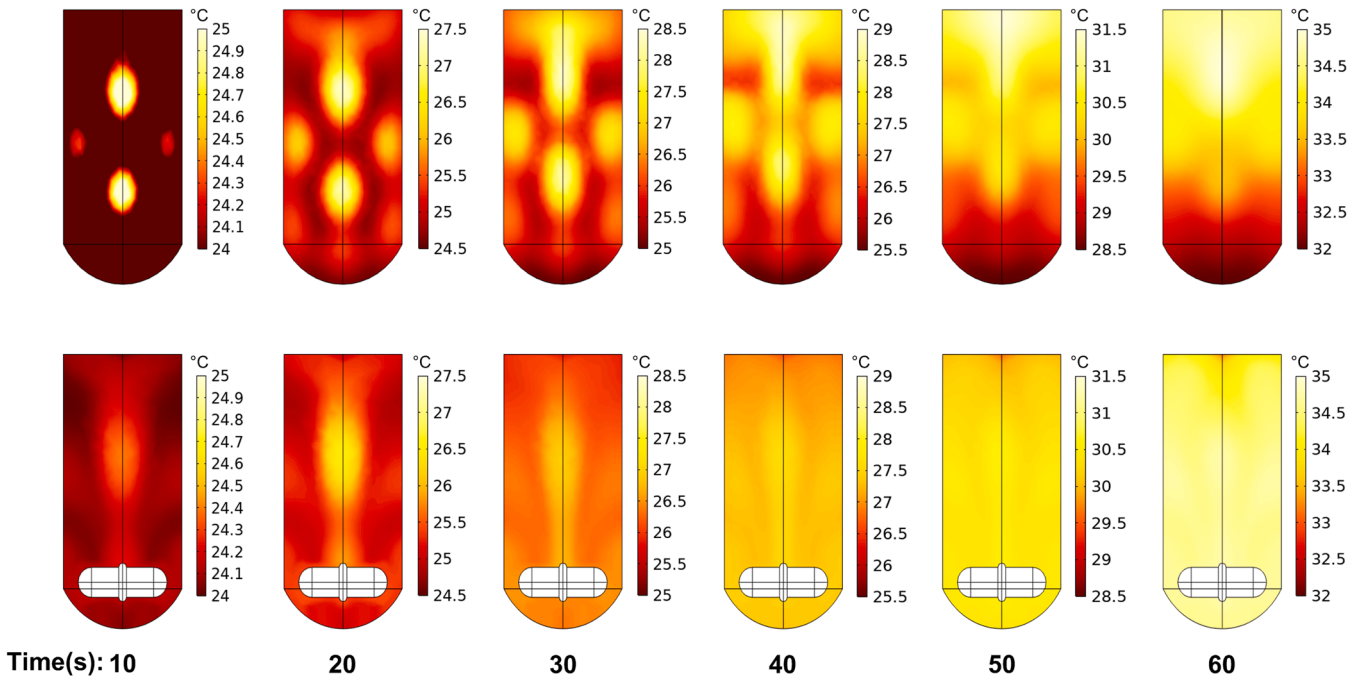

Fig. 13. Simulated Temperature contours of water filled to a height of 40 mm.

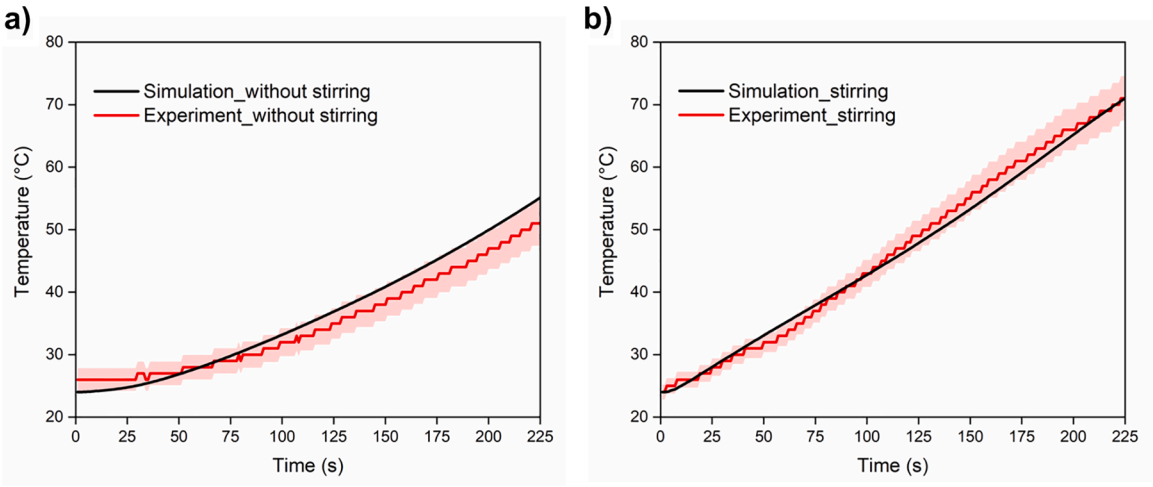

Fig. 14. Temperature prediction in (a) unstirred and (b) stirred water filled to a height of 40 mm.

of liquids under agitation during microwave heating, which will aid in microwave system design and process optimization. The proposed approach applies to any kind of motion within the reactor, such as mode stirrer, and enables mathematical prediction of microwave processing capability even with a local PC. This method significantly reduces convergence time by almost 600 times compared to conventional methods and eliminates the need for supercomputers under complex model conditions. The instantaneous simulation results open future research opportunities for integration with advanced technologies, such as neural network models to avoid deviations in the reaction in real-time.

CRediT authorship contribution statement

Bhupinder Singh: Writing – original draft, Validation, Software, Methodology, Investigation, Formal analysis, Conceptualization. **Samuel Hefford:** Writing – review & editing, Visualization, Conceptualization. **Enrique Sanchez-Perez:** Writing – review & editing, Visualization, Conceptualization. **Michael Barter:** Writing – review & editing, Visualization, Conceptualization. **Daniel R. Slocombe:** Writing – review & editing, Visualization, Project administration, Conceptualization. **Serena A. Cussen:** Writing – review & editing, Visualization, Project administration, Conceptualization. **Georgios Dimitrakis:** Writing – review & editing, Visualization, Supervision, Resources, Project administration, Conceptualization.

Declaration of competing interest

The authors declare that they have no known competing financial interests or personal relationships that could have appeared to influence the work reported in this paper.

Acknowledgement

The authors gratefully acknowledge the financial support received from Engineering and Physical Sciences Research Council (EPSRC), reference number EP/W018950/1.

Data availability

No data was used for the research described in the article.

References

[1] J.C. Atuonwu, S.A. Tassou, Quality assurance in microwave food processing and the enabling potentials of solid-state power generators: a review, J. Food Eng. 234 (2018) 1–15, https://doi.org/10.1016/j.jfoodeng.2018.04.009.
[2] D.E. Clark, D.C. Folz, J.K. West, Processing materials with microwave energy, 2000. www.elsevier.com/locate/msea.
[3] R.R. Mishra, A.K. Sharma, Microwave-material interaction phenomena: heating mechanisms, challenges and opportunities in material processing, Compos. Part A Appl. Sci. Manuf. 81 (2016) 78–97, https://doi.org/10.1016/j.compositesa.2015.10.035.
[4] Z. Peng, J.Y. Hwang, M. Andriese, Magnetic loss in microwave heating, Appl. Phys. Express 5 (2012), https://doi.org/10.1143/APEX.5.027304.
[5] J. Cheng, R. Roy, D. Agrawal, Experimental proof of major role of magnetic field losses in microwave heating of metal and metallic composites, n.d.
[6] A. de la Hoz, À. Díaz-Ortiz, A. Moreno, Microwaves in organic synthesis. Thermal and non-thermal microwave effects, Chem. Soc. Rev. 34 (2005) 164–178, https://doi.org/10.1039/b411438h.
[7] F. Wiesbrock, R. Hoogenboom, U.S. Schubert, Microwave-assisted polymer synthesis: state-of-the-art and future perspectives, Macromol. Rapid Commun. 25 (2004) 1739–1764, https://doi.org/10.1002/marc.200400313.
[8] G.D. Stefanidis, A.N. Muñoz, G.S.J. Sturm, A. Stankiewicz, A helicopter view of microwave application to chemical processes: reactions, separations, and equipment concepts, Rev. Chem. Eng. 30 (2014) 233–259, https://doi.org/10.1515/revce-2013-0033.
[9] B. Singh, S. Zafar, Microstructural and mechanical aspects of micrometric and nanometric Ni + 10 % Cr_7C_3 composite microwave clads, J. Compos. Mater. 55 (2021) 347–360, https://doi.org/10.1177/0021998320949617.
[10] A.J. Buttress, G. Hargreaves, A. Ilchev, T. Monti, A. Sklavounou, J. Katrib, P. Martin-Tanchereau, M.G. Unthank, D.J. Irvine, C.D. Dodds, Design and optimisation of a microwave reactor for kilo-scale polymer synthesis, Chem. Eng. Sci. 2 (2019), https://doi.org/10.1016/j.cesx.2019.100022.
[11] S. Najmi, B.C. Vance, E. Selvam, D. Huang, D.G. Vlachos, Controlling PET oligomers vs monomers via microwave-induced heating and swelling, Chem. Eng. J. 471 (2023), https://doi.org/10.1016/j.cej.2023.144712.
[12] F.E. Bedoya-Lora, V. Vásquez-Salgado, F.A. Vásquez, J.A. Calderón, Stable V-doped $LiMnPO_4$/C cathode material for Li-ion batteries produced by a fast and facile microwave-assisted synthesis, J. Alloys Compd. 938 (2023), https://doi.org/10.1016/j.jallcom.2022.168445.
[13] Y. Mao, A. Gerrow, E. Ray, N.D. Perez, K. Edler, B. Wolf, E. Binner, Lignin recovery from cocoa bean shell using microwave-assisted extraction and deep eutectic solvents, Bioresour. Technol. 372 (2023), https://doi.org/10.1016/j.biortech.2023.128680.
[14] M. Baker-Fales, T.Y. Chen, P. Bhalode, Z. Wang, D.G. Vlachos, Microwave enhancement of extractions and reactions in liquid–liquid biphasic systems, Chem. Eng. J. 476 (2023), https://doi.org/10.1016/j.cej.2023.146552.
[15] J.V. Laveda, B. Johnston, G.W. Paterson, P.J. Baker, M.G. Tucker, H.Y. Playford, K. M.O. Jensen, S.J.L. Billinge, S.A. Corr, Structure-property insights into nanostructured electrodes for Li-ion batteries from local structural and diffusional probes, J. Mater. Chem. A Mater. 6 (2017) 127–137, https://doi.org/10.1039/c7ta04400c.
[16] A. Porch, D. Slocombe, P.P. Edwards, Microwave absorption in powders of small conducting particles for heating applications, Phys. Chem. Chem. Phys. 15 (2013) 2757–2763, https://doi.org/10.1039/c2cp43310a.
[17] J. Joachim, C.A. Daunais, V. Bibeau, L. Heltai, B. Blais, A parallel and adaptative Nitsche immersed boundary method to simulate viscous mixing, J. Comput. Phys. 488 (2023), https://doi.org/10.1016/j.jcp.2023.112189.
[18] S.P. Yeong, M.C. Law, C.C. Vincent Lee, Y.S. Chan, Modelling batch microwave heating of water. IOP Conf Ser Mater Sci Eng, Institute of Physics Publishing, 2017, https://doi.org/10.1088/1757-899X/217/1/012035.
[19] Q. Zhang, T.H. Jackson, A. Ungan, Numerical modeling of microwave induced natural convection, n.d. www.elsevier.com/locate/ijhmt.
[20] G.L. Lee, M.C. Law, V.C.C. Lee, Numerical modelling of liquid heating and boiling phenomena under microwave irradiation using OpenFOAM, Int. J. Heat Mass Transf. 148 (2020), https://doi.org/10.1016/j.ijheatmasstransfer.2019.119096.
[21] G.S.J. Sturm, M.D. Verweij, T. Van Gerven, A.I. Stankiewicz, G.D. Stefanidis, On the effect of resonant microwave fields on temperature distribution in time and space, Int. J. Heat Mass Transf. 55 (2012) 3800–3811, https://doi.org/10.1016/j.ijheatmasstransfer.2012.02.065.
[22] T.Y. Chen, M. Baker-Fales, D.G. Vlachos, Operation and optimization of microwave-heated continuous-flow microfluidics, Ind. Eng. Chem. Res. 59 (2020) 10418–10427, https://doi.org/10.1021/acs.iecr.0c01650.
[23] S. Tuta, T.K. Palazoğlu, Finite element modeling of continuous-flow microwave heating of fluid foods and experimental validation, J. Food Eng. 192 (2017) 79–92, https://doi.org/10.1016/j.jfoodeng.2016.08.003.
[24] Y. Zhang, H. Yang, B. Yan, H. Zhu, W. Gao, J. Zhao, H. Zhang, W. Chen, D. Fan, Continuous flow microwave system with helical tubes for liquid food heating, J. Food Eng. 294 (2021), https://doi.org/10.1016/j.jfoodeng.2020.110409.
[25] S. Damilos, A.N.P. Radhakrishnan, G. Dimitrakis, J. Tang, A. Gavriilidis, Experimental and computational investigation of heat transfer in a microwave-assisted flow system, Chem. Eng. Process. - Process Intensif. 142 (2019), https://doi.org/10.1016/j.cep.2019.107537.
[26] S.S.R. Geedipalli, V. Rakesh, A.K. Datta, Modeling the heating uniformity contributed by a rotating turntable in microwave ovens, J. Food Eng. 82 (2007) 359–368, https://doi.org/10.1016/j.jfoodeng.2007.02.050.
[27] H. Topcam, O. Karatas, B. Erol, F. Erdogdu, Effect of rotation on temperature uniformity of microwave processed low - high viscosity liquids: a computational study with experimental validation, Innov. Food Sci. Emerg. Technol. 60 (2020), https://doi.org/10.1016/j.ifset.2020.102306.
[28] United States Patent, 2004.
[29] F. Szlivka, C. Hetyei, G. Fekete, I. Molnár, Comparison of mixing plane, frozen rotor, and sliding mesh methods on a counter-rotating dual-rotor wind turbine, Appl. Sci. (Switzerland) 13 (2023), https://doi.org/10.3390/app13158982.
[30] A. Corsini, G. Delibra, A.G. Sheard, A critical review of computational methods and their application in industrial fan design, ISRN Mech. Eng. 2013 (2013), https://doi.org/10.1155/2013/625175.
[31] A. Tamburini, A. Cipollina, G. Micale, A. Brucato, M. Ciofalo, CFD simulations of dense solid-liquid suspensions in baffled stirred tanks: prediction of suspension curves, Chem. Eng. J. 178 (2011) 324–341, https://doi.org/10.1016/j.cej.2011.10.016.
[32] G.L. Lane, M.P. Schwarz, G.M. Evans, Predicting gas-liquid flow in a mechanically stirred tank, n.d. www.elsevier.com/locate/apm.
[33] G. Montante, K.C. Lee, A. Brucato, M. Yianneskis, Numerical simulations of the dependency of flow pattern on impeller clearance in stirred vessels, 2001. www.elsevier.nl/locate/ces.
[34] W.Y. Kim, S. Senguttuvan, S.M. Kim, Effect of rotor spacing and duct diffusion angle on the aerodynamic performances of a counter-rotating ducted fan in hover mode, Processes 8 (2020) 1–14, https://doi.org/10.3390/pr8111338.
[35] B. Singh, S. Zafar, Understanding temperature characteristics during microwave cladding through process modeling and experimental investigation, CIRP J. Manuf. Sci. Technol. 37 (2022) 401–413, https://doi.org/10.1016/j.cirpj.2022.02.020.
[36] S. Chandrasekaran, S. Ramanathan, T. Basak, Microwave material processing—A review, AIChE J. 58 (2012) 330–363, https://doi.org/10.1002/aic.12766.
[37] C. Xu, J. Lan, J. Ye, Y. Yang, K. Huang, H. Zhu, Design of continuous-flow microwave reactor based on a leaky waveguide, Chem. Eng. J. 452 (2023), https://doi.org/10.1016/j.cej.2022.139690.
[38] O. Johnson Esua, D.W. Sun, C.K. Ajani, J.H. Cheng, K.M. Keener, Modelling of inactivation kinetics of *Escherichia coli* and *Listeria monocytogenes* on grass carp treated by combining ultrasound with plasma functionalized buffer, Ultrason. Sonochem. 88 (2022), https://doi.org/10.1016/j.ultsonch.2022.106086.
[39] T. Gao, D.W. Sun, Y. Tian, J. Ma, J.H. Cheng, Multiphysics modelling of constant power microwave heating of model juice, Int. J. Therm. Sci. 198 (2024), https://doi.org/10.1016/j.ijthermalsci.2024.108888.
[40] M. Frediani, G. Giachi, L. Rosi, P. Frediani, Synthesis and processing of biodegradable and bio-based polymers by microwave irradiation. Microwave Heating, InTech, 2011, https://doi.org/10.5772/23692.
[41] G. Halász, B. Gyüre, I.M. Jánosi, K.G. Szabó, T. Tél, Vortex flow generated by a magnetic stirrer, Am. J. Phys. 75 (2007) 1092–1098, https://doi.org/10.1119/1.2772287.
[42] G.B. Dudley, R. Richert, A.E. Stiegman, On the existence of and mechanism for microwave-specific reaction rate enhancement, Chem. Sci. 6 (2015) 2144–2152, https://doi.org/10.1039/c4sc03372h.
[43] A.Z. Fia, J. Amorim, Heating of biomass in microwave household oven—A numerical study, Energy 218 (2021), https://doi.org/10.1016/j.energy.2020.119472.